

# An Aircraft Icing Detection Method Based on Performance Data of Rotor

WU Yuan<sup>1,2\*</sup>, ZHU Dongyu<sup>1</sup>, XU Lingsong<sup>1</sup>, YU Lei<sup>1</sup>

1. Liaoning Provincial Key Laboratory of Aircraft Ice Protection, Aviation Industry Corporation of China Aerodynamics Research Institute, Shenyang 110034, P. R. China;

2. College of Aerospace Engineering, Nanjing University of Aeronautics and Astronautics, Nanjing 210016, P. R. China

(Received 21 February 2025; revised 8 April 2025; accepted 20 April 2025)

**Abstract:** Existing icing detection technologies face challenges when applied to small and medium-sized aircraft, especially electric vertical take-off and landing (eVTOL) aircraft that meet the needs of low-altitude economic development. This study proposes a data-driven icing detection method based on rotor performance evolution. Through dry-air baseline tests and dynamic icing comparative experiments (wind speed 0–30 m/s, rotational speed 0–3 000 r/min, collective pitch 0°–8°) of a 0.6 m rotor in the FL-61 icing wind tunnel, a multi-source heterogeneous dataset containing motion parameters, aerodynamic parameters, and icing state identifiers is constructed. An innovative signal processing architecture combining adaptive Kalman filtering and moving average cascading is adopted. And a comparative study is conducted on the performance of support vector machine (SVM), multilayer perceptron (MLP), and random forest (RF) algorithms, achieving real-time identification of icing states in rotating components. Experimental results demonstrate that the method exhibits a minimum detection latency of 6.9 s and 96% overall accuracy in reserved test cases, featuring low-latency and low false-alarm, providing a sensor-free lightweight solution for light/vertical takeoff and landing aircraft.

**Key words:** rotor; propeller; aircraft icing; icing detection; machine learning; support vector machine (SVM); multilayer perceptron (MLP)

**CLC number:** V244.15

**Document code:** A

**Article ID:** 1005-1120(2025)02-0212-14

## 0 Introduction

During flight, ice accretion on aircraft surfaces poses a significant threat to aviation safety. This is particularly critical to aircraft operating in cold regions. Ice formation on rotor blades or wing surfaces can lead to performance degradation, efficiency reduction, and even system failures. The accumulated ice increases the aircraft's weight and alters its aerodynamic characteristics, resulting in reduced lift, increased drag, and compromised flight stability and controllability. Furthermore, ice accretion may damage critical components and create potential risks to ground facilities and personnel. Airworthiness regulations stipulate that aircraft should either promptly exit the icing conditions or activate their anti-icing

and de-icing systems (IPS) based on their environmental suitability when encountering such conditions<sup>[1]</sup>. Consequently, developing efficient and reliable ice detection methodologies constitutes a crucial aspect of aviation safety assurance. The timely and accurate detection of aircraft icing status holds paramount importance for ensuring flight safety.

In recent years, significant progress has been made in aircraft icing detection research<sup>[2]</sup> compared to traditional visual observation, obstruction, and radiation methods<sup>[3]</sup>. For instance, the fiber-optic ice sensor<sup>[4-5]</sup>, and the ultrasonic pulse-echo technology-based ice sensor<sup>[6-7]</sup> have demonstrated excellent ice detection performance. Most of these studies focus on improving existing hardware systems

\*Corresponding author, E-mail address: wuyuanavicari@126.com.

**How to cite this article:** WU Yuan, ZHU Dongyu, XU Lingsong, et al. An aircraft icing detection method based on performance data of rotor[J]. Transactions of Nanjing University of Aeronautics and Astronautics, 2025, 42(2):212-225.

<http://dx.doi.org/10.16356/j.1005-1120.2025.02.006>

for ice detection. Since light aircraft and unmanned aerial vehicles (UAVs) face challenges in installing complex anti-icing/de-icing systems due to weight restrictions and cost considerations, simplifying detection devices and enhancing their practicality have become particularly crucial<sup>[8-9]</sup>. An increasing number of studies are exploring data-driven ice detection systems based on variations in flight performance.

Wind turbine blades share operational similarities with rotating aircraft components, offering valuable reference insights for icing detection research. Cheng<sup>[10]</sup> and Wang<sup>[11]</sup> proposed ice detection frameworks based on vibration signal spectral analysis and multi-source data fusion, respectively. Their models demonstrated superior robustness in low-temperature, high-humidity environments. Ye et al.<sup>[12]</sup> advanced the methodology by employing machine learning algorithms to process multidimensional sensor data from turbines, achieving simultaneous detection of ice thickness and spatial distribution. Notably, Kreutz et al.<sup>[13]</sup> developed a non-contact solution through RGB image analysis combined with convolutional neural network (CNN) for rotating blade icing detection, though such vision-based approaches exhibited applicability constraints in high-speed aircraft motion scenarios due to motion blur and dynamic resolution limitations.

In aircraft icing prediction, Yi et al.<sup>[14]</sup> developed a deep neural network-based model for ice shape prediction, establishing an end-to-end mapping between ice geometry features and flight parameters. Qu et al.<sup>[15]</sup> further proposed a generalized icing prediction framework applicable to arbitrary airfoils, achieving prediction errors within 5% by incorporating critical parameters such as boundary layer separation point location. Wang et al.<sup>[16]</sup> introduced a neural network-based intelligent method for flight risk prediction under icing conditions, demonstrating acceleration approaching three orders of magnitude compared to computational flight dynamics (CFD). Through systematic literature analysis, Yu et al.<sup>[17]</sup> concluded that current icing prediction technologies still face challenges in achieving high-precision real-time dynamic forecasting. They emphasized the substantial potential of data-driven ap-

proaches, advocating the integration of real-time monitoring data to develop more refined and personalized data-driven models.

Notably, practical aviation applications often prioritize rapid identification of critical aerodynamic parameters over full geometric reconstruction of ice shapes, offering a streamlined implementation pathway for engineering solutions.

For instance, Mckillip<sup>[18]</sup> proposed an indirect ice detection method by measuring changes in aircraft performance-related parameters. Deiler et al.<sup>[19]</sup> developed a novel robust ice detection method for early detection of ice-related performance degradation through flight data analysis of commercial aircraft, and their experimental validation demonstrated its significant potential in providing pilots with aircraft icing status. The methodology proposed by Caliskan et al.<sup>[20]</sup> integrated neural networks (NN) with the extended Kalman filter (EKF), achieving precise identification of icing conditions across various flight phases through analysis of simulated flight datasets from F-16 and A340 aircraft. This hybrid algorithm significantly enhances icing detection accuracy while substantially reducing system complexity, demonstrating particular suitability for aircraft platforms not equipped with conventional anti-icing/de-icing systems. The optimization-based approach leveraging existing system functionalities validates the technical feasibility of establishing an efficient detection framework without requiring additional hardware installations. However, it should be noted that the 48 000 training/validation/test datasets employed in the study were entirely generated through numerical simulations. Although the sheer volume of data and high-dimensional parameter characteristics ensure model reliability, they may potentially constrain its application potential in rapid-iteration, cost-sensitive engineering scenarios. Yue et al.<sup>[21]</sup> implemented long short-term memory (LSTM) neural networks for ice severity detection, which demonstrated that prolonged post-icing observation duration correlated with reduced prediction error in ice severity classification. Their findings indicated that at a 7 s detection window, over 90% of datasets exhibited detection error rates below 2%. As the

study primarily focused on ice severity assessment through data, with model accuracy as the sole evaluation metric, critical operational factors such as icing detection latency were not addressed in the methodology.

This paper proposes a novel aircraft icing detection methodology based on rotating component performance variation. This research establishes an ice identification framework through rotor aerodynamic characteristic evolution analysis. Its pivotal breakthrough lies in eliminating the stringent weight/space requirements imposed by traditional physical ice detectors and the dependence on massive datasets inherent to existing data-driven approaches. A dedicated rotor test rig is constructed in an icing wind tunnel to systematically acquire dynamic performance data under both dry-air and ice-accretion conditions. A lightweight machine learning algorithm specifically optimized for small-sample scenarios is employed for modeling analysis. Repeated validation trials and partitioned test dataset evaluations demonstrate that this approach holds detection accuracy while substantially reducing data requirements. This characteristic renders the method particularly suitable for conceptual verification phases of novel aircraft configurations, and engineering development scenarios under resource-constrained environments typical of small-medium enterprises. The methodology achieves an improved equilibrium between cost-effectiveness and engineering applicability, providing a novel technical pathway to enhance operational safety for light aircraft and unmanned aerial systems.

## 1 Experimental Setup

### 1.1 Wind tunnel description

The tests are carried out in the FL-61 icing wind tunnel of Aerodynamic Research Institute, Aviation Industry Corporation of China. As shown in Fig.1<sup>[22]</sup>, the FL-61 facility is a closed loop circuit refrigerated wind tunnel with a test section size of 0.6 m×0.6 m×2.7 m, driven by a 5 200 kW main compressor and a 2 500 kW auxiliary compressor. This facility could simulate the altitude effect

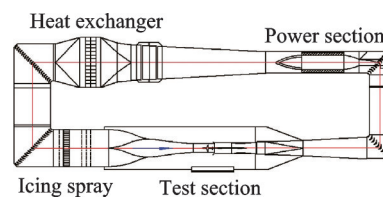


Fig.1 FL-61 icing wind tunnel<sup>[22]</sup>

on ice accretion up to 7 000 m. The maximum wind speed achievable in the test section is up to 240 m/s. Airflow refrigeration is obtained via a heat exchanger located upstream of the third corner. The minimum temperature achievable is  $-40\text{ }^{\circ}\text{C}$ . The accuracy is  $\pm 2\text{ }^{\circ}\text{C}$  when the temperature is below  $-30\text{ }^{\circ}\text{C}$  and  $\pm 0.5\text{ }^{\circ}\text{C}$  when it ranges from  $-30\text{ }^{\circ}\text{C}$  to  $5\text{ }^{\circ}\text{C}$ . The cloud uniformity of the test section is within  $\pm 20\%$ . The tunnel is equipped with a thermoelectric de-icing supply and hot-air de-icing system supply, which makes it suitable for ice protection system tests<sup>[23-24]</sup>.

The cloud control accuracy and uniformity of the FL-61 icing wind tunnel are calibrated and tested in accordance with SAE ARP 5905<sup>[25]</sup>. Its spray system can create cloud conditions that meet the median volume diameter (MVD) and liquid water content (LWC) requirements specified in Appendix C of FAR Part 25<sup>[1]</sup>. Specifically, located at the stable section of the FL-61 wind tunnel, the spray system is positioned approximately 8 m away from the test section. It has been determined that the droplets generated by this system and conveyed to the test section are present in a supercooled condition.

The wind tunnel is equipped with multiple test sections. To accommodate the spatial requirements for rotating component icing experiments, this study selects the open test section. Specifically, the original 0.6 m×0.6 m×2.7 m test section is extracted from the plenum chamber of the wind tunnel while retaining its corresponding nozzle and second throat. A support structure for the test article is installed at the original test section location.

According to flow-field calibration tests of the FL-61 icing wind tunnel, under conditions of  $Ma < 0.25$  and the standard atmospheric pressure, the core flow velocity uniformity region in the open test section covers a wide range. The Mach number fluctuation within the stream-wise model zone (from

100 mm to 1 350 mm downstream of the nozzle exit) remains within  $\pm 0.002$ , satisfying experimental requirements. Following the methodology established by Xu et al.<sup>[26]</sup>, the maximum dimensions and motion range of the test model are constrained to ensure stable and reliable experimental conditions while maintaining operational safety.

## 1.2 Rotor test rig of 0.6 m

The rotor test rig comprises a spindle tilting system, spindle power/force measurement system, spindle transmission system, and rotor control system (Fig.2). The spindle tilting system employs a motor-driven reducer and worm gear mechanism to adjust the rotor spindle's inclination angle. Mounted on the fixed end of a six-component balance serving as the structural support, this system interfaces with the balance as a critical load-bearing boundary. The spindle power/force measurement system integrates a spindle motor, a torque sensor, and a tachometer. The spindle transmission system consists of a drive shaft, bearing housing, and slip rings, installed on the floating end of the six-component balance via torque-balance diaphragm couplings. This assembly supports the combined weight and lift of the rotor hub, blades, and control system. The rotor control system features a swash-plate assembly, pitch push-rod components, and two synchronized electric cylinders for collective pitch adjustment.

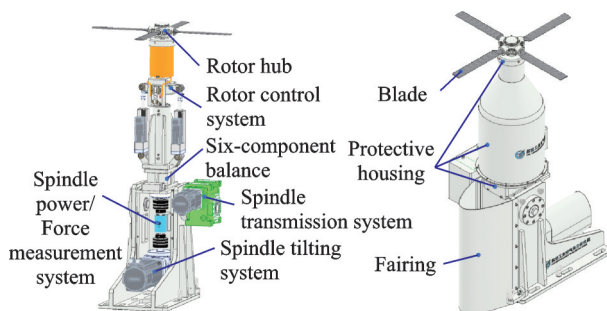


Fig.2 Schematic of rotor test rig configuration

The rig accommodates a 0.6 m diameter rotor (expandable to 1.2 m) with an adjustable collective pitch which is designed primarily for icing wind tunnel testing. A rigid hub with an internally integrated pitch adjustment mechanism enhances operational reliability in icing conditions while maintaining

strong scalability in rotating component configurations. All subsystems incorporate protective designs for sustained low-temperature/high-humidity operation, with critical areas receiving specialized sealing to prevent meltwater infiltration during anti/de-icing tests.

Key design specifications: (1) Aerodynamic configuration: NACA 23012 airfoil, 0.6 m rotor diameter (expandable to 1.2 m), four blades, maximum design speed 3 000 r/min; (2) tilt capability: Continuous spindle tilt adjustment ( $-90^{\circ}$ — $+5^{\circ}$ ) to support propeller testing requirements; (3) pitch range: Collective pitch adjustable from  $-2^{\circ}$  to  $+12^{\circ}$ ; (4) instrumentation: Integrated force/torque measurement and blade anti-icing test capabilities.

Deployed in the FL-61 wind tunnel open test section, this rig enables icing and electrothermal anti/de-icing tests on rotating components (rotors, propellers, tilt-rotors, etc.), capturing pre/post-icing spindle load characteristics and torque data. Ground tests confirm tilt/pitch repeatability  $<0.1^{\circ}$ , speed control accuracy  $<0.1\%$ , and vibration-free operation across the entire revolutions per minute (RMP) envelope.

## 2 Rotor Icing Performance Variation Tests

This study establishes a multi-source heterogeneous data fusion-based rotor icing feature acquisition system with the following technical implementation pathway: A rotor test rig is installed in the FL-61 icing wind tunnel open test section to obtain rotor performance evolution data through dry-air baseline tests and dynamic icing comparative experiments. The data acquisition system employs a distributed architecture design, maintaining real-time communication with the rotor control unit, FL-61 wind tunnel measurement/control system, and spray system to synchronously collect three groups of critical parameters: (1) Rotor motion parameters (commanded/actual rotational speed, pitch angle, tilt angle, output torque); (2) aerodynamic environment parameters (velocity, total temperature, total pres-

sure) ; (3) icing state identification parameters (spray system activation status represented by Boolean 0/1 values for non-icing/icing conditions).

Notably, high-precision clock synchronization technology is implemented to achieve temporal alignment between wind tunnel spray valve operations and rotor platform status parameters, thereby constructing physically meaningful supervised learning labels that provide a reliable data foundation for subsequent machine learning-based icing detection algorithm development.

The rotor icing performance test procedure designed in this study is as follows:

(1) Install the rotor test rig in the open test section of the FL-61 icing wind tunnel; after leveling, perform operational status inspection and evaluation of the test rig; calibrate the tilt angle and collective pitch angle.

(2) Inspect the surface condition of rotor blades; remove surface contaminants and foreign objects.

(3) Start the main compressor of the wind tunnel; adjust the wind speed to the target value and maintain stability.

(4) Activate the rotor test rig control system; adjust the rotor to the predetermined tilt angle and the collective pitch angle through the servo motor control system; start the main motor and gradually increase the rotational speed to the set value.

(5) After the spray system reaches a stable working state, activate the spray system and automatically control its on/off operation according to the predetermined sequence.

(6) After the test, open the wind tunnel chamber; record the ice shape characteristics on the rotor surface; collect icing data.

Safety constraint is that limited by the test rig design, the rotor rotational speed must be reset to zero before adjusting the tilt angle and the collective pitch angle.

The test conditions are sets as shown in Table 1.

**Table 1 Rotor icing performance test matrix**

Case	Velocity/ ( $\text{m}\cdot\text{s}^{-1}$ )	Temperature/ $^{\circ}\text{C}$	Tilt angle/ ( $^{\circ}$ )	Pitch angle/ ( $^{\circ}$ )	Rotational speed/ ( $\text{r}\cdot\text{min}^{-1}$ )	Spray duration/s
1	0	-8.6	-6	8	0—1 000	—
2	0	-8.6	-6	8	2 000—3 000	—
3	10	-6	-6	8	0—2 700	—
4	30	>0	-6	8	2 000	—
5	0—30	-8.4	-6—0	0—8	1 600—2 500	—
6	30	-8.6	-6	8	2 000	600
7	30	-8.6	-6	8	2 000	600
8	30	-8.6	-6	8	2 000	600
9	30	-8.6	-6	8	2 000	300
10	30	-7.5	-6	8	2 000	300
11	30	-7	-6	8	2 000	120
12	30	-7	-6	8	2 000	120
13	30	-7.7	-6	8	2 000	120
14	30	-7.5	-6	8	2 200	120
15	30	-7.3	-6	8	2 200	120
16	30	-7.3	-6	8	2 500	120

Cases 1—5 are dry air baseline tests. The spray system remains closed throughout each test. By adjusting parameters including the wind speed (0—30 m/s), the tilt angle ( $-6^{\circ}$ — $0^{\circ}$ ), the collec-

tive pitch angle ( $0$ — $8^{\circ}$ ), and the rotational speed ( $0$ — $3\ 000$  r/min), the system investigates the sensitivity of rotor aerodynamic parameters to multivariate inputs.

Cases 6—16 are icing tests and repeatability tests. Multiple baseline tests (primarily with a varying rotational speed) are conducted using the dry air test method before each spray. The spray system operates in partial nozzle mode (36/121 nozzles activated). The water pressure is set to 100 kPa and the air pressure to 160 kPa. Cloud parameters estimated based on previous spray system control studies<sup>[14]</sup> are  $MVD = 21 \mu\text{m}$  and  $LWC = 1.2 \text{ g/m}^3$ .

### 3 Data Preprocessing and Analysis

#### 3.1 Data preprocessing

This study develops a systematic six-stage data preprocessing framework (Fig.3). The system achieves feature enhancement and data optimization through multi-dimensional signal processing, effectively addressing critical challenges in rotor icing detection tasks including noise interference, insufficient feature representation, and sample imbalance.

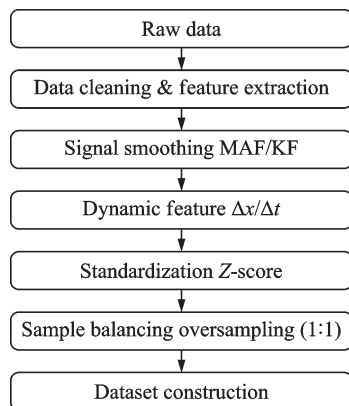


Fig.3 Six-stage data preprocessing framework

This structured data preprocessing workflow comprises six key technical stages.

(1) **Data cleaning & feature extraction:** Manual data analysis removes invalid or low-quality data. Through physical mechanism-based analysis of rotor performance variations before/after icing,  $m$  key feature parameters (e.g., wind speed, torque, rotational speed) are extracted to construct feature matrix  $\mathbf{X} \in \mathbf{R}^{n \times m}$ , with corresponding icing state labels  $y \in \{0, 1\}^n$  from system outputs, establishing a supervised learning benchmark.

(2) **Signal smoothing:** The high-frequency noise in sensor measurements is eliminated using

sliding window moving average filter (MAF) or Kalman filter (KF)<sup>[27]</sup>.

MAF is expressed as

$$\bar{x}_t = \frac{1}{N} \sum_{i=t-N+1}^t x_i \quad (1)$$

where  $N$  is the window width.

The KF is a recursive algorithm that eliminates the need for historical data storage while dynamically quantifying state uncertainties through covariance matrices. It achieves optimal measurement estimation by fusing predictions from system models with actual sensor measurements through weighted averaging—A process that inherently suppresses stochastic noise. The weighting coefficients governing this fusion are determined by the process noise covariance  $\mathbf{Q}$  and measurement noise covariance  $\mathbf{R}$ . Specifically, an increased  $\mathbf{Q}$  prioritizes trust in real-time measurements, whereas a higher  $\mathbf{R}$  favors model-based predictions.

(3) **Dynamic feature construction:** Considering limited sample size, temporal dynamic characteristics are enhanced through differential rate features without complex time-series algorithms

$$\Delta x_t = x_t - x_{t-\Delta t} \quad (2)$$

where  $\Delta t$  is the time interval. This doubles feature dimensions, generating augmented matrix  $\mathbf{X}' \in \mathbf{R}^{n \times 2m}$  containing original features and first-order differences.

(4) **Data standardization:** Z-score normalization eliminates unit discrepancies

$$z = \frac{x - \mu}{\sigma} \quad (3)$$

where  $\mu$  and  $\sigma$  denote the training set mean and the standard deviation, respectively. Standardization parameters are persistently stored to ensure the consistency across testing, real-time icing detection, and training phases.

(5) **Sample balancing:** This step is implemented via the improved random resampling algorithm. Let  $n_1$  and  $n_0$  represent positive/negative sample counts, respectively, with the balancing constraint

$$\min(|n_1 - (n_0 + \delta)|) \quad (4)$$

Setting  $\delta = 0$ , and the final balanced dataset maximizes sample retention while maintaining positive/negative ratio at strict 1:1.

(6) Dataset construction: Temporal correlations are eliminated through random permutation, splitting data into 8:2 training-test sets. This partitioning strategy, validated by K-fold cross-validation, ensures independence of data distributions.

### 3.2 Support vector machine

Support vector machine (SVM) is a supervised learning algorithm based on statistical learning theory. Its core principle involves constructing optimal hyper-planes or hyper-surfaces to achieve data classification or regression. For linearly separable problems, SVM enhances model generalization capability by maximizing the classification margin, i.e., the minimum distance between two classes of samples to the hyperplane. For nonlinear problems, kernel functions, e.g., Gaussian kernel, polynomial kernel, are employed to map original features into high-dimensional spaces for linear separability. SVM demonstrates superior performance in small-sample and high-dimensional data scenarios while effectively mitigating overfitting.

This study selects SVM primarily for two reasons.

(1) Limited data availability: Experimental data are obtained from a small number of wind tunnel tests, resulting in a limited sample size. Through the structural risk minimization principle, SVM optimizes models in small-sample scenarios by fully leveraging limited data to extract classification boundaries, thereby avoiding underfitting or overfitting caused by insufficient data.

(2) Feature separability: Experimental results reveal significant feature differences between icing conditions and normal operating conditions. Specifically, post-icing torque variation rates of rotating components under undisturbed conditions exhibit distinct patterns compared to normal flight states and rotational speed transition phases. SVM efficiently captures such nonlinearly separable features through kernel tricks, constructing robust classification decision boundaries.

The classifier is implemented using the SVC class from Python's scikit-learn library<sup>[28]</sup>, with the radial basis function (RBF) kernel to balance model

complexity and classification performance.

The implementation involves solving the following primal optimization problem

$$\min_{\mathbf{w}, b} \frac{1}{2} |\mathbf{w}|^2 + C \sum_{i=1}^n \xi_i \quad (5)$$

subject to

$$\begin{aligned} y_i(\mathbf{w} \cdot \phi(\mathbf{x}_i) + b) &\geq 1 - \xi_i \\ \xi_i &\geq 0; \quad i = 1, 2, \dots, n \end{aligned} \quad (6)$$

where  $\mathbf{w}$  is the weight vector determining the hyperplane orientation;  $b$  the bias term controlling the hyperplane's offset from the origin;  $C$  the penalty parameter balancing margin size and support vector count;  $\xi_i$  the slack variable allowing classification error;  $\mathbf{x}_i$  the feature vector mapped via kernel function; and  $y_i \in \{+1, -1\}$  the class label of sample  $\mathbf{x}_i$ .

To handle nonlinearly separable data, SVC employs kernel functions  $K(\mathbf{x}_i, \mathbf{x}_j)$  for high-dimensional mapping. This study uses the RBF kernel

$$K(\mathbf{x}_i, \mathbf{x}_j) = \exp(-\gamma |\mathbf{x}_i - \mathbf{x}_j|^2) \quad (7)$$

By introducing Lagrange multipliers  $\alpha_i$ , the primal problem is transformed into the dual problem

$$\max_{\alpha} \sum_{i=1}^n \alpha_i - \frac{1}{2} \sum_{i,j=1}^n y_i y_j \alpha_i \alpha_j K(\mathbf{x}_i, \mathbf{x}_j) \quad (8)$$

subject to

$$0 \leq \alpha_i \leq C, \quad \sum_{i=1}^n \alpha_i y_i = 0 \quad (9)$$

After solving for  $\alpha_i$ , the weight vector and bias term are computed as

$$\begin{cases} \mathbf{w} = \sum_{i=1}^n \alpha_i y_i \phi(\mathbf{x}_i) \\ b = y_i - \mathbf{w} \cdot \phi(\mathbf{x}_i) \end{cases} \quad (10)$$

for support vectors.

### 3.3 Random forest

Random forest (RF)<sup>[29]</sup> is an ensemble learning-based supervised algorithm that enhances classification performance by combining multiple decision trees. For binary classification tasks, each decision tree independently classifies samples, and the final prediction is determined through a "majority voting" mechanism (i.e., the class with the highest votes is selected as the result). Its core principles include sample perturbation (bootstrap sampling) and feature perturbation (random selection of feature sub-

sets), which reduce over-fitting risks in individual trees while improving model generalization.

The core splitting criteria in RF rely on two impurity metrics: The Gini index and information gain. These metrics quantify the purity variation of data before and after node splitting, thereby guiding optimal feature selection during decision tree construction.

The Gini index evaluates node impurity by measuring the dispersion of class distribution. Its principle proclaims that if all samples in a node belong to a single class (ideal purity), the Gini index reaches its minimum value of 0. Conversely, it attains the maximum value when class distributions are uniform. The mathematical definition is

$$\mathcal{G}(t) = 1 - \sum_{i=1}^M \left( \frac{N_i^{(t)}}{N^{(t)}} \right)^2 \quad (11)$$

where  $M$  denotes the total number of classes ( $M=2$  for binary classification);  $N^{(t)}$  the total number of samples in node  $t$ ; and  $N_i^{(t)}$  the count of class  $i$  samples in node  $t$ . During feature selection, the algorithm prioritizes splits that maximize the weighted reduction in Gini impurity across child nodes.

Information gain utilizes Shannon entropy to assess feature importance by measuring the reduction in system disorder after splitting. The entropy is defined as

$$\mathcal{H}(t) = - \sum_{i=1}^M \left( \frac{N_i^{(t)}}{N^{(t)}} \right) \log_2 \left( \frac{N_i^{(t)}}{N^{(t)}} \right) \quad (12)$$

Information gain is calculated as the difference between the parent node entropy and the weighted sum of child node entropies

$$\text{IG}(S, A) = \mathcal{H}(S) - \sum_{k=1}^K \frac{N^{(S_k)}}{N^{(S)}} \mathcal{H}(S_k) \quad (13)$$

where  $S$  denotes the parent node sample set;  $A$  the candidate feature for splitting;  $K$  the number of splitting branches for feature  $A$ ; and  $S_k$  corresponds to the sample set of the  $k$ th child node. Higher information gain values indicate greater discriminative power of feature  $A$  for class separation.

### 3.4 Multilayer perceptron

The multilayer perceptron (MLP)<sup>[30]</sup> is a feed-forward neural network architecture capable of learning complex nonlinear decision boundaries for binary

classification tasks. It stacks multiple fully connected layers, including an input layer, one or more hidden layers with activation functions, and an output layer. For binary classification, the output layer typically uses a single neuron with a sigmoid activation function to map predictions to probabilistic outputs within  $[0, 1]$ . Training involves optimizing weights and biases through backpropagation to minimize cross-entropy loss, enabling the model to capture hierarchical feature representations.

Given the input features  $\mathbf{x}$ , the output of the  $l$ th hidden layer is computed as

$$\mathbf{h}^{(l)} = \sigma(\mathbf{W}^{(l)}\mathbf{h}^{(l-1)} + \mathbf{b}^{(l)}) \quad (14)$$

where  $\mathbf{W}^{(l)}$  and  $\mathbf{b}^{(l)}$  are the weight matrix and bias vector of layer  $l$ , respectively; and  $\sigma$  denotes a non-linear activation function (e.g., ReLU for hidden layers).

The final prediction  $\hat{y}$  is generated via the sigmoid activation

$$\hat{y} = \sigma(\mathbf{W}^{(L)}\mathbf{h}^{(L-1)} + \mathbf{b}^{(L)}), \sigma(z) = \frac{1}{1 + e^{-z}} \quad (15)$$

where  $\hat{y}$  represents the estimated probability of the positive class.

Binary cross-entropy loss measures prediction error

$$\mathcal{L} = - \frac{1}{N} \sum_{i=1}^N [y_i \ln \hat{y}_i + (1 - y_i) \ln (1 - \hat{y}_i)] \quad (16)$$

where  $y_i \in \{0, 1\}$  is the true label and  $\hat{y}_i$  the predicted probability.

### 3.5 Hyperparameter optimization

In the field of machine learning model optimization, the random search has gained significant attention as an efficient automated hyperparameter optimization method. Compared with the traditional grid search, this approach employs a probability distribution-based sampling mechanism in parameter space, which significantly enhances computational efficiency while maintaining optimization effectiveness. The core principle involves uniform distribution sampling of hyperparameter combinations, effectively circumventing the curse of dimensionality encountered by grid search in high-dimensional spaces. Empirical studies by Bergstra et al.<sup>[31]</sup> demonstrate that when the objective function exhibits low effective dimensionality characteristics, random search can

identify superior solutions with 95% probability within 60 iterations compared to 500 iterations of the grid search. This method proves particular advantages for hyperparameter optimization in complex models such as neural networks, with theoretical bounds on convergence speed proven to exhibit sublinear relationships with parameter space dimensionality.

This study employs the random search algorithm to systematically optimize the hyperparameter spaces of three distinct models, SVM, RF, and MLP. We construct uniform distribution sampling spaces for each model's critical hyperparameters, including kernel coefficients and penalty factors for SVM, tree depth and feature sampling rates for RF, as well as hidden layer configurations and activation functions for MLP. By setting 50 search iterations with five-fold cross-validation accuracy as the optimization objective, the automated parameter tuning is implemented through Randomized-SearchCV module from Python's scikit-learn library<sup>[28]</sup>.

### 3.6 Quantitative evaluation framework

To systematically optimize model hyperparameter configurations and comprehensively evaluate

the performance differences among multiple classification algorithms, including RF, SVM, and MLP, this study establishes a quantitative evaluation framework for binary classification problems. By employing the confusion matrix (Table 2) as the core analytical tool and integrating a multi-dimensional evaluation index system derived from it, encompassing values of accuracy, precision, recall, F1-score, receiver operating characteristic (ROC) curves, and area under curve (AUC) (Table 3), the framework effectively reveals distinct characteristics of different models in terms of feature recognition, class discrimination, and error type distribution. This methodological approach provides robust data support for model selection and optimization.

**Table 2 Confusion matrix**

Confusion matrix	Definition
True positive(TP)	Number of positive samples correctly predicted as positive
False positive(FP)	Number of negative samples incorrectly predicted as positive (Type I error)
True negative(TN)	Number of negative samples correctly predicted as negative
False negative(FN)	Number of positive samples incorrectly predicted as negative (Type II error)

**Table 3 Evaluation index system**

Evaluation index	Formula	Meaning
Accuracy	$\frac{TP + TN}{TP + TN + FP + FN}$	Proportion of all correct predictions
Precision	$\frac{TP}{TP + FP}$	Proportion of true positives among predicted positives (reduces FP)
Recall	$\frac{TP}{TP + FN}$	Proportion of true positives correctly identified (reduces FN)
F1-score	$2 \cdot \frac{\text{Precision} \cdot \text{Recall}}{\text{Precision} + \text{Recall}}$	Harmonic mean of precision and recall, balancing both
ROC curve	Plot of TPR (y-axis) vs. FPR (x-axis) across thresholds	Visualizes model's ability to distinguish classes at various thresholds
AUC	Area under the ROC curve	Quantifies overall class separation ability; higher values indicate better performance

Given the stringent requirements for aviation icing detectors to achieve both low false positive rates (FPR) and low false negative rates (FNR), this study systematically evaluates three core metrics for icing state detection: Precision, recall, and F1-

score. Notably, the F1-score is selected as the objective function for automatic hyperparameter optimization, as it effectively balances the trade-off between precision and recall, thereby mitigating detection bias caused by single-metric optimization. Fur-

thermore, to ensure real-time responsiveness of in-flight icing warning systems, this research innovatively proposes the “icing detection latency” metric, defined as the time difference between the actual physical icing onset moment and the algorithm’s first valid detection moment. This latency metric is integrated into a multi-dimensional performance evaluation framework, establishing a novel paradigm that combines reliability and timeliness for the design of detection algorithms in aviation safety-critical systems.

To evaluate model effectiveness, one test run is randomly reserved as an independent test set to validate the model’s generalization capability on unseen data. Through this methodology, the SVM model achieves high-precision classification under small-sample conditions, providing a reliable theoretical foundation for icing state detection.

## 4 Results and Discussion

Experimental observations reveal that under specific test conditions, the rotor surface demonstrates typical mix ice accretion characteristics influenced by blade geometric scale effects. Notably, the ice morphology exhibits a pronounced gradient distribution along the spanwise direction: The tip region (0—1 chord length from blade tip) predominantly features glaze ice formation, while the root region (3—4 chord lengths from blade tip) displays characteristic rime ice morphology. The ice thickness distribution along both spanwise and chordwise directions shows marked gradient characteristics, with the growth rate demonstrating nonlinear attenuation when the distance from the blade tip is less than 50 mm.

Comparative analysis of different spray durations (300 s/ 600 s) indicates quantitative variations in ice thickness magnitudes while maintaining consistent spatial distribution patterns. Through continuous monitoring of ice surface morphology evolution, it can be inferred that no ice shedding phenomena are observed during the experimental process. This consistency in spatial distribution characteristics across varying exposure times suggests stable

ice accretion mechanisms under the tested parametric conditions.

Torque, as a critical parameter characterizing the dynamic characteristics of rotor systems, exhibits significant dynamic response features under icing conditions. Fig.4 reveals the coupling relationships between torque parameters and rotor operational parameters (rotational speed, collective pitch angle, and tilt angle) through experimental data from Case 5. The test results demonstrate that during flight attitude adjustments, the collective pitch angle and rotational speed modifications exert dominant influence on torque variations, while the tilt angle changes show limited impact. Notably, torque fluctuations induced by operational commands manifest immediate response characteristics, whereas ice accumulation effects produce gradual evolution of torque changes. This temporal contrast between command-driven and ice-induced torque variations is clearly demonstrated in the time-domain analysis presented in Fig.5.

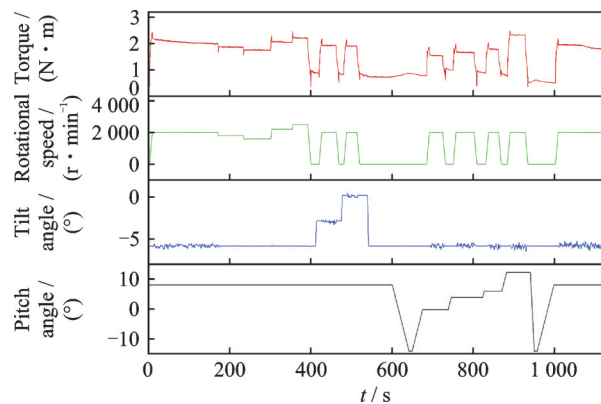


Fig.4 Torque variations induced by rotational speed, tilt angle, and collective pitch angle adjustments in Case 5

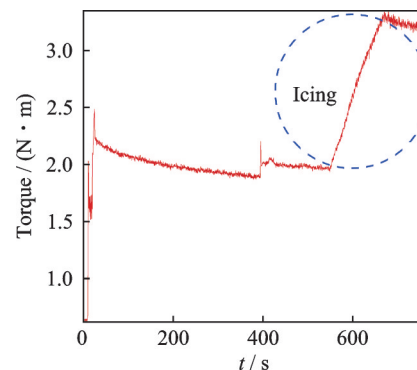


Fig.5 Torque changes following spray activation

This study employs supervised learning methods to develop a predictive model, achieving equivalent characterization of the complex physical processes in rotor icing through feature engineering. Distinct from traditional mechanism-based modeling approaches, the proposed algorithm constructs a feature space: By introducing an adaptive weight allocation mechanism, it transforms the nonlinear relationships between rotor dynamic parameters and icing processes into quantifiable feature parameter combinations. During the data preprocessing phase (as detailed in Section 3), a stratified random sampling strategy is implemented for dataset partitioning, with Case 13 reserved as an independent validation set for real-time performance testing.

#### 4.1 Signal smoothing

This study reveals the comprehensive advantages of various filtering schemes through multi-dimensional comparative analysis (Fig.6). The standalone KF demonstrates robust performance in amplitude fluctuation suppression. Although the MAF achieves comparable visual smoothness to KF, it incurs dynamic feature detail loss. The cascaded filtering scheme (KF+MAF) optimizes data smoothness metrics, but exhibits more pronounced dynamic hysteresis compared to the standalone MAF approach.

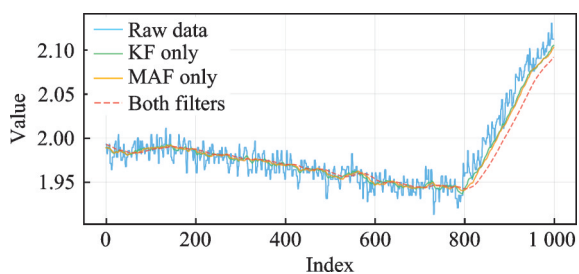


Fig.6 Prediction performance without dynamic feature consideration

Preliminary theoretical analysis suggests that standalone KF or MAF schemes exhibit potential advantages in temporal tracking metrics. However, empirical analysis of the predictive model reveals critical paradoxical phenomena (Fig.7). Although single-filter configurations enhance temporal track-

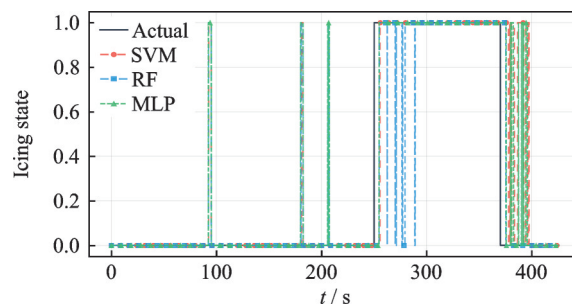


Fig.7 Icing detection performance using standalone KF schemes

ing capability, they induce systematic degradation in model prediction efficacy, specifically manifesting a statistically significant increase in a false alarm rate.

Through systematic evaluation, this research establishes an optimized hybrid filtering architecture: A KF core with process noise covariance  $Q=0.001$  and measurement noise covariance  $R=0.3$ , complemented by a secondary VAF with 40-sample window size. This configuration achieves optimal balance between data fidelity and prediction reliability.

#### 4.2 Hyperparameter optimization analysis

Through automated hyperparameter optimization via random search, three classical machine learning models obtain domain-adapted optimal configurations. For MLP, the architecture employs a dual hidden-layer topology (20, 10) with tanh activation, achieving optimized nonlinear representation through intermediate-dimensional hierarchical feature extraction. The L2 regularization coefficient  $\alpha=0.0098$  and batch size 128 establish stability control in gradient updates. The RF configuration embodies deep ensemble learning strategy, where 450 decision trees with a maximum depth of 17 construct high-complexity feature interaction space, while dynamic sample splitting thresholds ( $\text{min\_samples\_split}=0.325$ ,  $\text{min\_samples\_leaf}=0.1$ ) enable precise overfitting control. The SVM parameters demonstrate strong regularization characteristics. The significantly elevated penalty coefficient  $C=21.83$  indicates strict suppression of classification errors, combined with RBF kernel ( $\gamma=1.56$ ) enabling optimal hyperplane construction in high-dimensional feature space.

Table 4 systematically compares the performance of MLP, RF, and SVM models on four core classification metrics (precision, recall, F1-score, and accuracy) when tested with optimized hyperparameters on a reserved test dataset containing 11 981 samples. MLP and SVM exhibit statistical equivalence across all four metrics, with both models achieving comprehensive performance metrics surpassing the 0.97 threshold, demonstrating significantly superior performance relative to the RF model. The RF model shows notable deficiencies in recall (0.77) and F1-score (0.86), indicating inadequate feature capture for positive class samples in its learning mechanism.

**Table 4** Classification metrics tested with optimized hyperparameters

Model	Precision	Recall	F1-score	Accuracy
MLP	0.98	0.97	0.97	0.973 3
RF	0.96	0.77	0.86	0.870 2
SVM	0.97	0.97	0.97	0.971 1

### 4.3 Icing detection performance

To systematically replicate real-world flight conditions, particularly sudden icing meteorological encounters during single-flight operations as previously established, this study reserves Case 13 as final validation data. As illustrated in Fig.8, all models demonstrate initial alert suppression at 250.3 s flight time when spray initiation occurs under simulated icing conditions. As detailed in Fig.9, the SVM methodology detects icing formation and triggers alerts 6.9 s post-initiation, followed by MLP detection with 0.1 s later. Notably, the RF approach exhibits a critical 40 s latency in proper response activation. This renders it operationally unacceptable.

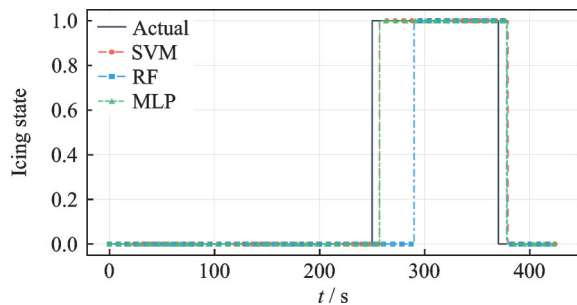


Fig.8 Final icing detection performance comparison

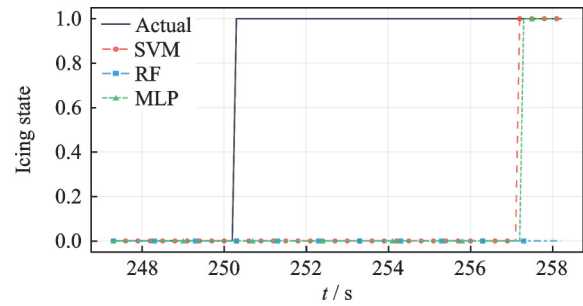


Fig.9 Icing detection latency during icing cloud encounters

Under current sample size constraints and data processing protocols, SVM and MLP demonstrate statistical equivalence in engineering applicability, maintaining low algorithmic response latencies and false-positive rates that satisfy aviation safety thresholds. Conversely, RF's performance metrics significantly underperform operational requirements, establishing its impracticality for real-time aircraft icing detection systems.

## 5 Conclusions

This study develops a data-driven rotor icing detection method based on FL-61 wind tunnel rotor icing performance variation tests, achieving effective identification and analysis of rotor icing characteristics. The main conclusions are as follows.

(1) The icing detection method based on rotating component performance parameter variations demonstrates engineering feasibility, with experimental validation confirming the physical rationality of this technical approach.

(2) Under limited sample conditions, SVM and MLP exhibit excellent prediction performance with minimal resource consumption, meeting real-time monitoring requirements for rotating component icing. Conversely, RF is unacceptable.

(3) Independent test sample verification shows the method maintains prediction latency under 7 s, with overall test cycle prediction accuracy exceeding 96%.

It should be noted that the current research is limited by experimental conditions, and the operational coverage and the sample size of the dataset require enhancement. Subsequent work will expand data dimensions through multi-condition wind tun-

nel tests combined with numerical simulations.

This improvement will significantly enhance the engineering applicability of this technology in lightweight and vertical takeoff and landing aircraft icing protection systems.

## References

- [1] Federal Aviation Administration. Part 25-airworthiness standards: Transport category airplanes[S]. [S. l.]: FAA, 2014.
- [2] CHEN Yong, KONG Weiliang, LIU Hong. Challenge of aircraft design under operational conditions of supercooled large water droplet icing[J]. *Acta Aeronautica et Astronautica Sinica*, 2023, 44(1): 626973. (in Chinese)
- [3] ZHANG Jie, ZHOU Lei, ZHANG Hong, et al. Aircraft icing detection technology[J]. *Chinese Journal of Scientific Instrument*, 2006, 27(12): 1578-1586. (in Chinese)
- [4] LI Wei, CHEN Yingchun, ZHANG Miao, et al. Novel icing detection system based on optical waveguide technique[J]. *Instrument Technique and Sensor*, 2009(12): 85-87. (in Chinese)
- [5] WANG Qiang, YI Xian, WANG Wen, et al. Cloud parameter calculation and ice shape prediction method based on fiber optic icing detection: CN202210224054.0[P]. 2023-04-11. (in Chinese)
- [6] WANG Y, WANG Y, LI W, et al. Study on freezing characteristics of the surface water film over glaze ice by using an ultrasonic pulse-echo technique[J]. *Ultrasonics*, 2022, 126: 106804.
- [7] WANG Yan, WANG Yuan, ZHU Chengxiang, et al. Simulation and experimental study of aircraft icing detection sensor by resonant[J]. *Journal of Nanjing University of Aeronautics & Astronautics*, 2022, 54(2): 267-273. (in Chinese)
- [8] LØW-HANSEN B, HANN R, STOVNER B N, et al. UAV icing: A survey of recent developments in ice detection methods[J]. *IFAC-PapersOnLine*, 2023, 56(2): 10727-10739.
- [9] YAN S, OPAZO T, PALACIOS J, et al. Experimental evaluation of multi-rotor uav operation under icing conditions[C]//*Proceedings of the Vertical Flight Society 74th Annual Forum*. Phoenix, USA: The Vertical Flight Society, 2018: 1-12.
- [10] CHENG Xu. Data-driven blade icing detection of wind turbines[D]. Tianjin: Tianjin University of Technology, 2021. (in Chinese)
- [11] WANG Feifan. The research on data-driven icing detection method for wind turbine blade[D]. Zhuzhou: Hunan University of Technology, 2025. (in Chinese)
- [12] YE F, EZZAT A A. Icing detection and prediction for wind turbines using multivariate sensor data and machine learning[J]. *Renewable Energy*, 2024, 231: 120879.
- [13] KREUTZ M, ALLA A A, EISENSTADT A, et al. Ice detection on rotor blades of wind turbines using RGB images and convolutional neural networks[J]. *Procedia CIRP*, 2020, 93: 1292-1297.
- [14] YI Xian, WANG Qiang, CHAI Congcong, et al. Prediction model of aircraft icing based on deep neural network[J]. *Transactions of Nanjing University of Aeronautics and Astronautics*, 2021, 38(4): 535-544.
- [15] QU Jingguo, PENG Bo, YI Xian, et al. Icing prediction method for arbitrary airfoil using deep neural networks[J]. *Acta Aerodynamica Sinica*, 2023, 41(7): 48-55. (in Chinese)
- [16] WANG G Z, XU H J, PEI B B. An intelligent approach for flight risk prediction under icing conditions[J]. *Chinese Journal of Aeronautics*, 2023, 36(6): 109-127.
- [17] YU Sirui, SONG Mengjie, SHEN Jun, et al. Research progress on icing characteristic prediction technologies for low temperature stationary and moving surfaces[J]. *Journal of Harbin Institute of Technology*, 2024, 56(10): 150-168. (in Chinese)
- [18] MCKILLIP R M. Aircraft icing detection system: US6304194[P]. 2001-10-16.
- [19] DEILER C, FEZANS N. Performance-based ice detection methodology[J]. *Journal of Aircraft*, 2020, 57(2): 209-223.
- [20] CALISKAN F, HAJIYEV C. A review of in-flight detection and identification of aircraft icing and reconfigurable control[J]. *Progress in Aerospace Sciences*, 2013, 60: 12-34.
- [21] YUE T, WANG X L, WANG B, et al. Design of ice tolerance flight envelope protection control system for UAV based on LSTM neural network for detecting icing severity[J]. *Drones*, 2025, 9(1): 63.
- [22] ZHAO Huanyu, YU Lei, ZHU Dongyu, et al. Superhydrophobic surface application of runback icing elimination and anti-icing power reduction and icing wind tunnel test[J]. *Transactions of Nanjing University of Aeronautics and Astronautics*, 2023, 40(6): 678-687.
- [23] YU L, WU Y, ZHAO H Y, et al. A study on the sensitivities of an ice protection system combining thermoelectric and superhydrophobic coating to icing envi-

- ronment parameters[J]. Applied Sciences, 2023, 13(11): 6607.
- [24] WU Yuan, YU Lei, LI Si, et al. Study on the effect of icing wind tunnel spray system control on liquid water content[C]//Proceedings of the 6th China Aeronautical Science and Technology Conference. Singapore: Springer Nature Singapore, 2024: 670-680.
- [25] AC-9C Aircraft Icing Technology Committee. Calibration and acceptance of icing wind tunnels: ARP5905A [S]. [S.l.]: SAE International, 2025.
- [26] XU Lingsong, WU Yuan, LIU Haihan, et al. A test device and method for large-sized specimens based on small-scale icing wind tunnel: CN202410240506.3 [P]. 2024-06-14. (in Chinese)
- [27] KALMAN R E. A new approach to linear filtering and prediction problems[J]. Journal of Basic Engineering, 1960, 82(1): 35-45.
- [28] PEDREGOSA F, VAROQUAUX G, GRAMFORT A, et al. Scikit-learn: Machine learning in python[J]. Journal of Machine Learning Research, 2011, 12: 2825-2830.
- [29] BREIMAN L. Random forests[J]. Machine Learning, 2001, 45(1): 5-32.
- [30] GOODFELLOW I, BENGIO Y, COURVILLE A. Deep learning[M]. Cambridge, USA: The MIT Press, 2016.
- [31] BERGSTRA J, BENGIO Y. Random search for hyper-parameter optimization[J]. Journal of Machine Learning Research, 2012, 13: 281-305.

**Acknowledgements** This work was supported in part by

the National Key R&D Program of China (No.2022YFE02-03700), and the Aeronautical Science Foundation of China (No. 2023Z010027001). The authors would like to acknowledge the following people for their assistance: GUO Jin, LIU Nan, JIANG Xinkai, ZHANG Jinlong, and NIE Xin.

#### Author

**The first/corresponding author** Mr. WU Yuan received his B.S. degree in mechanics engineering from Beihang University in 2010 and M.S. degree in fluid mechanics engineering from Chinese Aeronautical Establishment in 2016. From 2010 to present, he has been with Aerodynamics Research Institute, Aviation Industry Corporation of China, where he is currently a senior engineer and manager of Liaoning Provincial Key Laboratory for Aircraft Ice Protection. His research has focused on aircraft icing, which includes convection heat transfer, roughness on iced surface, ice adhesion, micro-scale droplet dynamics and thermodynamics, and icing protection of rotating parts.

**Author contributions** Mr. WU Yuan designed the study, developed the code, conducted the analysis, interpreted the results and wrote the manuscript. Mr. ZHU Dongyu coordinated the technical roadmap, and contributed to all phases of the study. Mr. XU Lingsong proposed the innovative design of the rotor test rig, and participated in experimental validation and data processing. Mr. YU Lei contributed to the discussion and background of the study. All authors commented on the manuscript draft and approved the submission.

**Competing interests** The authors declare no competing interests.

(Production Editor: ZHANG Bei)

## 基于旋翼性能变化的飞机结冰探测方法研究

吴 渊<sup>1,2</sup>, 朱东宇<sup>1</sup>, 许岭松<sup>1</sup>, 于 雷<sup>1</sup>

(1. 中航工业空气动力研究院辽宁省飞行器防除冰重点实验室, 沈阳 110034, 中国;

2. 南京航空航天大学航空学院, 南京 210016, 中国)

**摘要:** 现有的结冰探测技术在应用于中小型飞行器, 特别是适应低空经济发展需求的电动垂直起降飞机时, 难以同时满足载重限制和适应飞行姿态变化的需求, 无法精准、高效地完成结冰探测任务。本研究提出一种基于旋翼性能变化的数据驱动结冰探测方法, 通过FL-61结冰风洞中0.6 m旋翼的干空气基准测试与动态结冰对比实验(风速0~30 m/s, 转速0~3 000 r/min, 桨距角0°~8°), 构建了包含运动参数、气动参数与结冰状态标识的多源异构数据集。创新性地采用自适应卡尔曼滤波与移动平均级联的信号处理架构, 对比研究支持向量机、多层感知器和随机森林等多种算法的性能, 实现了旋转部件结冰状态的实时辨识。试验研究表明: 该方法在保留测试案例中展现出最低6.9 s的检测延迟与96%的整体准确率, 具有低延迟低误报率等特点, 为轻型/垂直起降航空器提供了无需额外传感器的轻量化解决方案。

**关键词:** 旋翼; 螺旋桨; 飞机结冰; 结冰探测; 机器学习; 支持向量机; 多层感知机